*Progress In Electromagnetics Research M, Vol. 98, 11–20, 2020*

# A CPW-Fed Dual-band MIMO Antenna with Enhanced Isolation for 5G Application

**Chengzhu Du* and Zhuolin Zhao**

**Abstract**—In this paper, a dual-band Multiple Input Multiple Output (MIMO) antenna for fifth-generation (5G) band (3.3–3.6 GHz and 4.8–5.0 GHz) is presented. The proposed MIMO antenna fed by coplanar waveguide (CPW) contains two symmetric antenna elements with two inverted L-shaped stubs. High isolation is successfully acquired by adopting a double-Y-shaped stub and partial ground plane. To obtain compactness, the antenna printed on an FR4 substrate has two triangle corners cut off. To study the performance, the antenna is simulated by Ansoft HFSS 13.0, and then fabricated and tested. The measurement results demonstrate that the antenna has achieved impedance bandwidths ($S_{11} < -10$ dB) of 790 MHz (3.08–3.87 GHz) and 880 MHz (4.7–5.58 GHz) with fractional bandwidths of 22.7% and 15.8%, respectively, which covers 3.45/4.9 GHz 5G bands. Meanwhile, the measurement results exhibit an enhanced isolation more than 20 dB, a low envelope correlation coefficient (ECC) below 0.001, an average gain better than 2 dB, and a stable radiation pattern within operation bands. In addition, the parameters including efficiency, DG, CCL, MEG, and TARC are also analysed. The simulated and measured results indicate that the proposed MIMO antenna can be applied to 5G communication system.

## 1. INTRODUCTION

Nowadays, mobile 5G communication system has become a promising technique for its advantages of higher speed and wider frequency bandwidth than traditional communication systems. The sub-6 GHz, as a key element in 5G frequency bands, combines the original 2G, 3G, and 4G frequency bands [1]. Meanwhile, MIMO system has attracted extensive attention in these years for its benefits including low multipath fading effects, increased channel capacity, and high transmission rate compared to the single antenna communication system. However, it is hard to achieve a high isolation and maintain a compact size at the same time in the process of design [2]. Therefore, how to decouple between antenna elements has been a critical problem in the process of design. In addition, designing a MIMO antenna fulfilling operation for 5G application is a challenge as well.

The design of isolation mechanism plays a key part in the whole process because the antenna element cannot be independent within a limited space. So far, numerous MIMO antennas with dual-band have been proposed in [3–14]. In [3], the method of defected ground structure (DGS) combined with meander-lines results in the isolation increasing to above 15 dB by disturbing the surface current flow. In [4], a meandering-line resonator expanding from the ground plane is responsible for obtaining the decrease of mutual coupling to below $-25$ dB. It is reported in [5] that a meandering resonant stub extending from the ground plane and an inverted T-shaped slot notched on the ground plane are adopted to the MIMO antenna for WLAN application to reduce the lower and upper band coupling to more than 15 dB respectively. It is reported in [6] that a combination of DGS and asymmetrical

*Received 12 August 2020, Accepted 6 October 2020, Scheduled 27 October 2020*

* Corresponding author: Chengzhu Du (duchengzhu@163.com).

The authors are with the College of Electronics and Information Engineering, Shanghai University of Electric Power, Shanghai 200090, China.

coplanar strip (ACPS) is adopted to ease mutual coupling of the dual-band MIMO antenna to above 20 dB. It is reported in [7] that MIMO antenna has a decoupling network inserted between two arranged symmetric dual-band antenna elements to obtain a high isolation over 30 dB. However, these MIMO antennas mentioned usually have large area.

A dual-band MIMO antenna working at WLAN bands is reported in [8], which uses a metal strip connected between elements as a neutralization line and a ⊢-shaped stub as an isolation stub to enhance the isolation to exceed 20 dB. High isolation has been achieved by a decoupling network with a combination of a broad slot and two symmetric narrow slots to disrupt the current distribution, realizing the decrease of the mutual coupling to below −20 dB in [9]. In [10], a T-shaped connecting line added between antenna elements and two slots notched on the ground plane are used to acquire high isolation. The T-shaped connecting line acts as a neuralization line to counteract the current coupling, and two slots help to disturb and restrain the current flow to the other port. In [11], an elliptical slot working as a band-stop filter and a rectangular parasitic strip as an isolation stub to suppress the surface waves are employed to realize a high isolation. It is reported that a MIMO antenna of dual-bands with improved mutual coupling of lower and upper bands by 30.61 dB is achieved by combining DGS and asymmetrical coplanar strip (ACPS) in [12]. In [13], by means of setting the feeders of antenna elements orthogonally to each other, mutual coupling below −22.5 dB between antenna elements is achieved. In [14], a T-shaped connecting line functioning as a short stub-loaded resonator (SSLR) is involved between dual-band antenna elements to increase the isolation to more than 19 dB. However, all of the dual-band MIMO antennas mentioned above are fed by coaxial feed or microstrip feed, which are not easy to integrate with circuits.

In this paper, a dual-band MIMO antenna based on CPW-feed with the characteristic of an enhanced isolation is presented for 5G communication system. The antenna is made up of two elements printed orthogonally on a hexagon substrate. The antenna originates from two inverted L-shaped radiators. A high isolation is successfully acquired by adding a novel double-Y-shaped stub. The proposed antenna covers 3.45/4.9 GHz 5G bands, and the isolation is better than 20 dB. The performances of antenna including $S$-parameters, radiation patterns, envelope correlation efficient (ECC), diversity gain (DG), gain, efficiency, channel capacity loss (CCL), mean effective gain (MEG), and total active reflection coefficient (TARC) have been simulated and tested. It is summarized from the results that the dual-band MIMO antenna for 5G application with an enhanced isolation has been successfully realized.

## 2. ANTENNA DESIGN AND ANALYSIS

### 2.1. Antenna Geometry

The configuration of the proposed antenna is illustrated in Figure 1(a), and the prototype of the fabricated antenna is presented in Figure 1(b). The antenna is fabricated on a 0.8-mm-thick FR4 dielectric substrate with a relative dielectric constant of 4.4 and loss tangent of 0.02. The two antenna elements, depicted as Ant_1 and Ant_2, respectively, use two inverted L-shaped radiators of a quarter wavelength to generate two operation bands (3.3–3.6 GHz and 4.8–5.0 GHz). The software of Ansoft HFSS 13.0 is employed for the simulation of performance and optimization of dimensions in the process of design.

### 2.2. Design Process

Figure 2 presents the process of the antenna design, starting from Ant A through Ant B and Ant C to Ant D. The $S$-parameters simulated in every step are plotted in Figure 3.

Originally, the single antenna element operating in two frequency bands (3.45/4.9 GHz) is realized by two inverted L-shaped stubs. In Ant A, two elements of the same structure are arranged orthogonally. It can be observed from Figure 3 that the return loss ($S_{11}$) of Ant A is lower than −10 dB over 3.3–3.9 GHz and 4.7–5.0 GHz while mutual coupling is very serious over the operation bands.

Then, in Ant B, a double-Y-shaped stub acting as a reflective component is added in the location of the diagonal line of the square substrate [15]. It can be proved that minimum isolation is increased

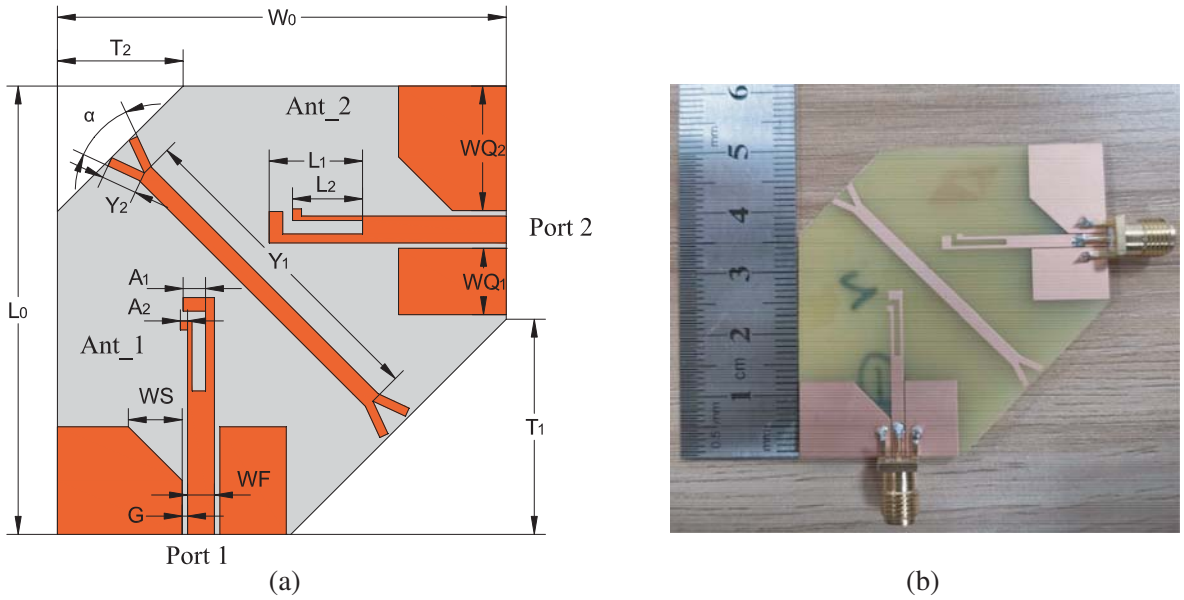


**Figure 1.** (a) Geometry of the proposed MIMO antenna. (b) Prototype of fabricated antenna. Dimensions (in mm): $L_0 = 50$, $W_0 = 50$, $T_1 = 24$, $T_2 = 14$, $G = 0.2$, $WS = 6$, $WQ_1 = 8.3$, $WQ_2 = 14.8$, $WF = 2$, $Y_1 = 36$, $Y_2 = 4$, $LF = 16$, $L_1 = 10.4$, $L_2 = 8$, $A_1 = 1.7$, $A_2 = 0.5$.

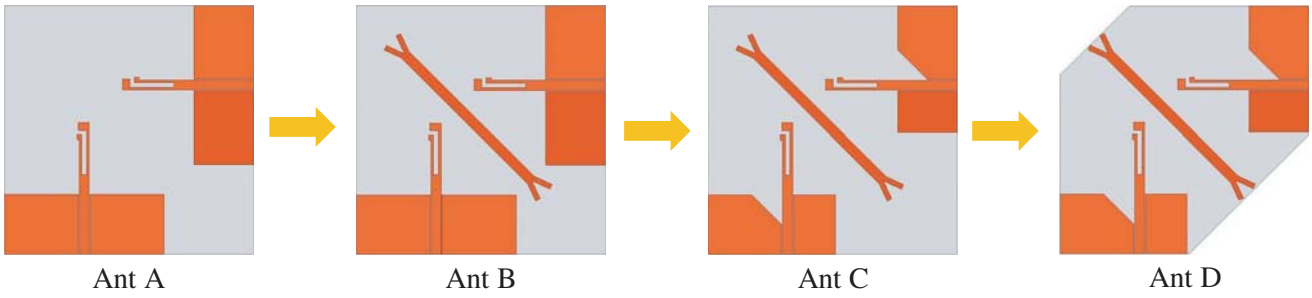


**Figure 2.** Process of antenna design.

by 7 dB within operating bands. However, impedance bandwidths are shrunk covering 3.2–3.6 GHz and 4.7–4.8 GHz.

In addition, in Ant C, the introduction of a defect ground structure, cutting off a triangle corner on the ground planes, helps to broad the impedance bandwidth. As a result, impedance bandwidth is expanded greatly covering 3.2–3.8 GHz and 4.7–6.0 GHz, and the isolation is improved as well with the value of $S_{12}$ reduced to below −22 dB and −28 dB at 3.45 GHz band and at 4.9 GHz band, respectively.

Finally, in Ant D, two triangles are cut off from the square substrate to obtain a small size. It is noted that the reduction of substrate has little effect on the performance of Ant D compared with Ant C.

### 2.3. Parametric Study

To have a further research on the decoupling structure as presented above, the analysis of the dimension has been done as follows.

It is shown in Figure 4 that with the extension of the length of the double-Y-shaped stub ($Y_1$), the isolation at the lower band turns worse with the upper band isolation hitting the peak level at $Y_1 = 37$ mm, maintaining better than 20 dB within operation bands, while the resonant frequencies of both the bands are nearly unaffected.

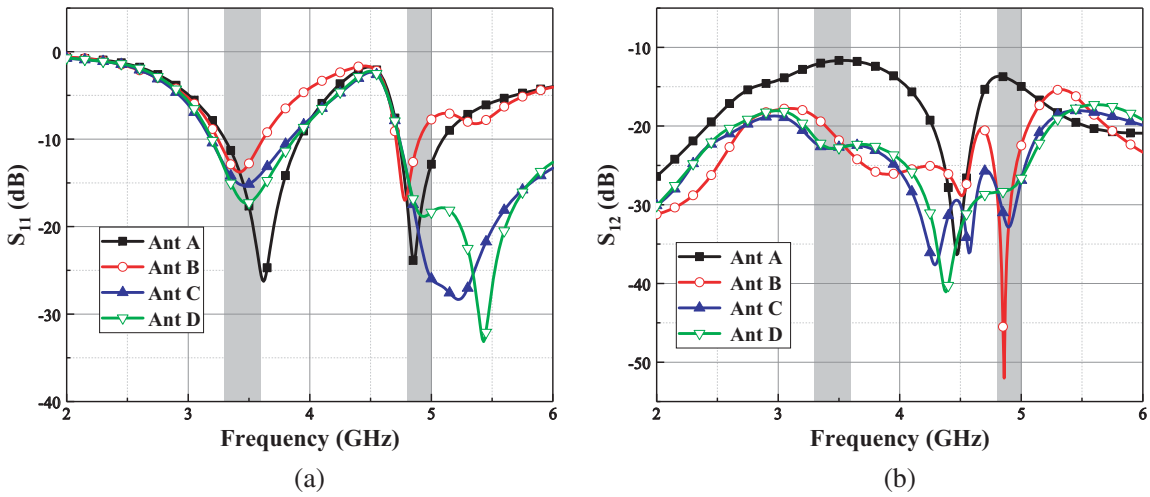


**Figure 3.** Simulated $S$-parameters (a) $S_{11}$ and (b) $S_{12}$ of antenna evolution.

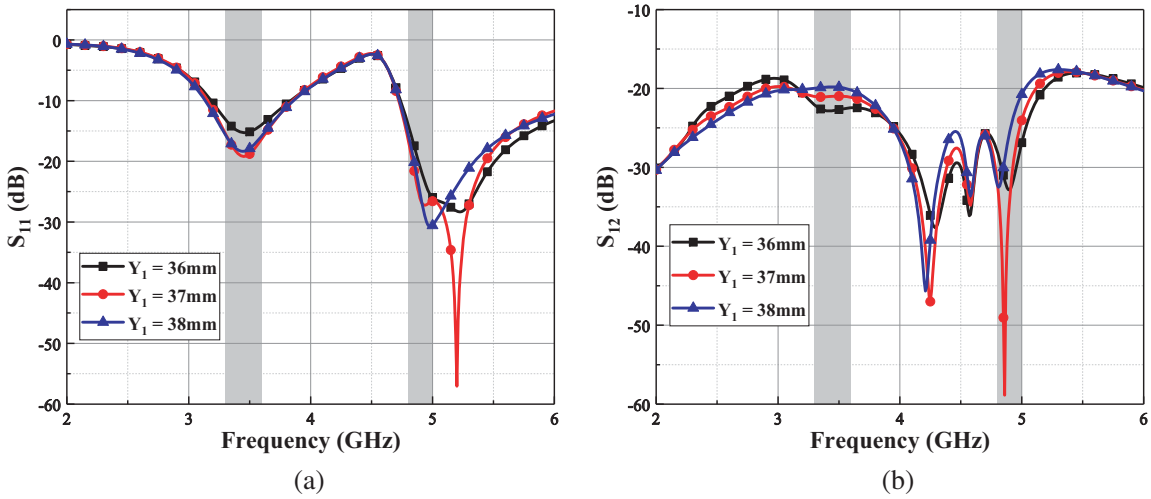


**Figure 4.** Simulated (a) $S_{11}$ and (b) $S_{12}$ of the proposed MIMO antenna for various $Y_1$.

## 2.4. Current Distribution

For the sake of analysing the decoupling mechanism visually, the surface current distributions of Ant A, together with Ant C and Ant D at 3.45 GHz and 4.9 GHz, are simulated by keeping Port 1 excited and Port 2 matched with 50-Ω load, which are shown in Figure 5 and Figure 6.

It is exhibited in Figure 5(a) that there exists a large amount of current coupling from Ant_1 to Ant_2 at 3.45 GHz in Ant A, resulting in poor isolation. Figure 5(b) shows that when the double-Y-shaped stub is added and the structure of ground plane modified in Ant C, a mass of surface current is reflected to the decoupling structure. Compared with Ant C, the current distribution of Ant D has little change, which proves that the reduction of the size of the substrate has little effect on the current distribution.

Similarly, Figure 6 shows the current distributions of Ant A, Ant C, and Ant D at 4.9 GHz. As mentioned above, the introduction of the double-Y-shaped stub contributes significantly to the diminution of mutual coupling at 4.9 GHz. A less quantity of current is coupled to Port 2 in Ant D compared with Ant A. In addition, reducing the size of the substrate has little influence on the current distribution with the comparison of Ant C and Ant D.

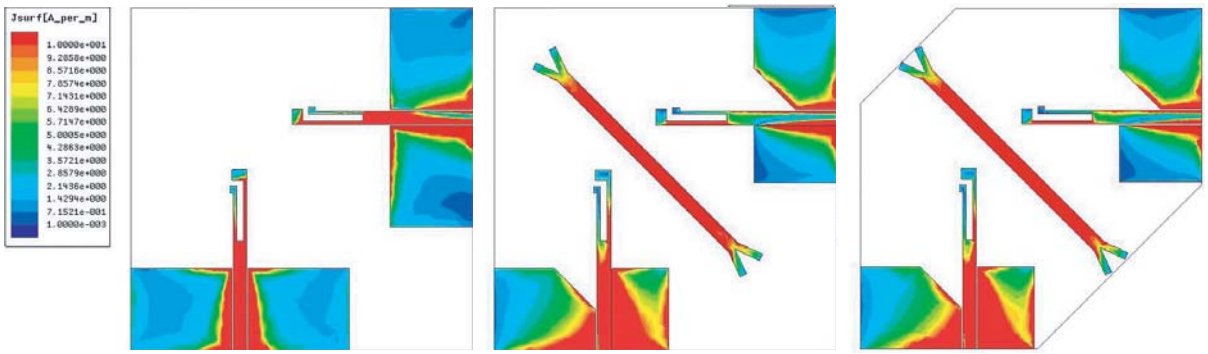


**Figure 5.** Simulated surface current distribution on (a) Ant A, (b) Ant C, and (c) Ant D at 3.45 GHz.

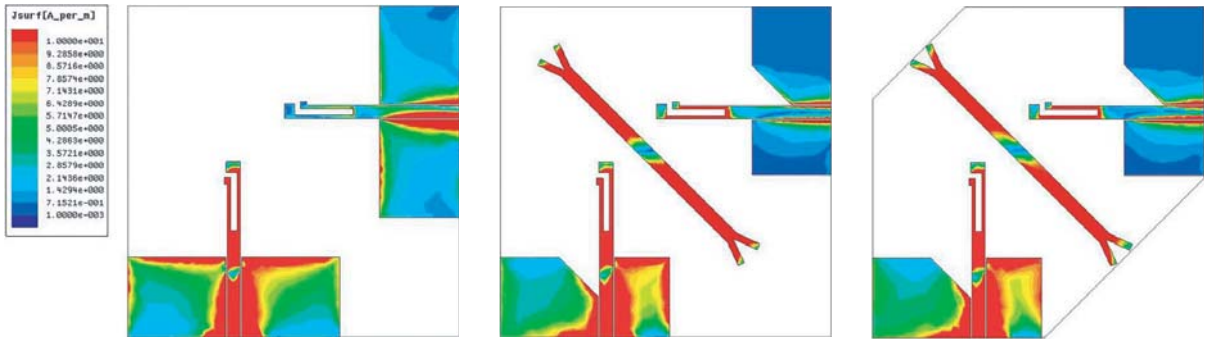


**Figure 6.** Simulated surface current distribution on (a) Ant A, (b) Ant C, and (c) Ant D at 4.9 GHz.

## 3. RESULTS AND DISCUSSION

### 3.1. *S*-Parameters

To certify the proposal above, a prototype of the proposed antenna is fabricated and tested. The measurement results are obtained by using Agilent PNA-L N5230A Network Analyzer. Figure 7 shows the curves of measured and simulated results, including $S$-parameters of $S_{11}$ and $S_{12}$. It is exhibited that the measured results coincide with simulation ones greatly within operating bands. The measured impedance bandwidths are 3.08–3.87 GHz and 4.76–5.58 GHz with a fractional bandwidth of 22.7% and 15.8%, respectively. From transmission curves, it can be illustrated that $S_{12}$ is below $-20$ dB and $-25$ dB at 3.45 GHz band and 4.9 GHz band, respectively.

### 3.2. Radiation Pattern

To obtain an intuitive insight of the radiation mechanism of the antenna, both the simulated and measured far field normalized radiation patterns in $H$-plane and $E$-plane at 3.45 GHz and 4.9 GHz are presented in Figure 8. For the reason of absolutely symmetrical arrangement and the same structure of the antenna elements, the measured results are obtained by keeping Port 1 excited and Port 2 matched with 50-$\Omega$ load. As can be seen from the polar curves, measured radiation patterns nearly agree with simulated results which appear omnidirectional. Compared with coplanar polarization, the cross-polar level of the antenna is lower than the coplanar polar level at the same frequency expect a few points. However, there exists a little discrepancy between measured and simulated results, which can attribute to the uncertainty of testing environment and fabrication tolerance.

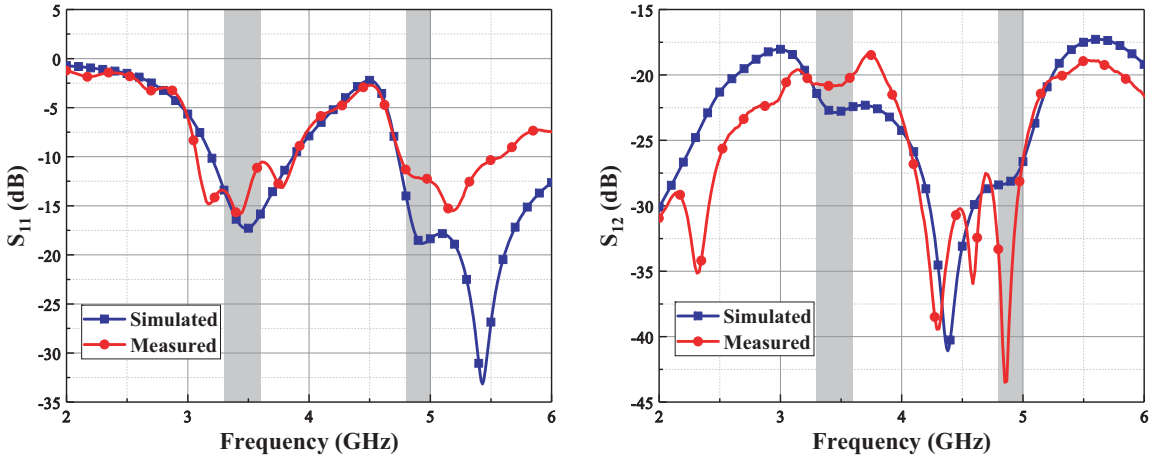


**Figure 7.** Simulated and measured (a) $S_{11}$ and (b) $S_{12}$ of the proposed antenna.

### 3.3. Envelope Correlation Coefficient and Diversity Gain

During the analysis of MIMO antenna, envelope correlation coefficient (ECC) is considered as a valuable parameter to evaluate the degree of signal fading or diversity skill of MIMO antenna. ECC has a negative correlation with channel capacity, which means that a large channel capacity reflects a low level of ECC. The approximative expression of ECC for MIMO antenna is calculated as [16]:

$$ECC = \frac{|\ S_{11}^* S_{12} + S_{21}^* S_{22}\ |^2}{(1 - |\ S_{11}\ |^2 - |\ S_{21}\ |^2)(1 - |\ S_{22}\ |^2 - |\ S_{12}\ |)^2} \tag{1}$$

It is exhibited in Figure 9 that the simulated and measured values of ECC are below 0.001 within the operating bands while the practically acceptable range is less than 0.5, which proves that the MIMO antenna possesses a good performance.

Similarly, diversity gain (DG) acts as the other index to assess the characteristic of MIMO antenna. The value of DG can be calculated as [17]:

$$DG = 10\sqrt{1 - (ECC)^2} \tag{2}$$

Figure 10 plots the simulated and measured curves of DG, showing that the proposed MIMO antenna possesses a high level of DG (better than 9.9).

### 3.4. Gain

The gain curves are presented in Figure 11. It is exhibited obviously that the simulated average gains are around 3 dB and 4 dB for 3.45 GHz band and 4.9 GHz band, respectively, while the measured gains are near 3 dB and 2 dB for 3.45 GHz band and 4.9 GHz band, respectively. The difference between simulated and measured results is primarily caused by the uncertainty of the test environment, SMA connector loss, and fabrication tolerance.

### 3.5. Channel Capacity Loss and Mean Effective Gain

The parameter of channel capacity loss (CCL) is defined as the maximum extent of available data transmission rate before the occurrence of significant signal fading. It is necessary to evaluate the limit capacity of data transmission rate of MIMO antenna. The calculation of CCL is given as follows [18]:

$$CCL = -\log_2 \det\left(\Psi^R\right) \tag{3}$$

where $\Psi^R = \begin{bmatrix} \Psi_{11} & \Psi_{12} \\ \Psi_{21} & \Psi_{22} \end{bmatrix}$, $\Psi_{ii} = 1 - (|S_{ii}|^2 + |S_{ij}|^2)$ and $\Psi_{ij} = -(S_{ii}^* S_{ij} + S_{ji}^* S_{ij})$.

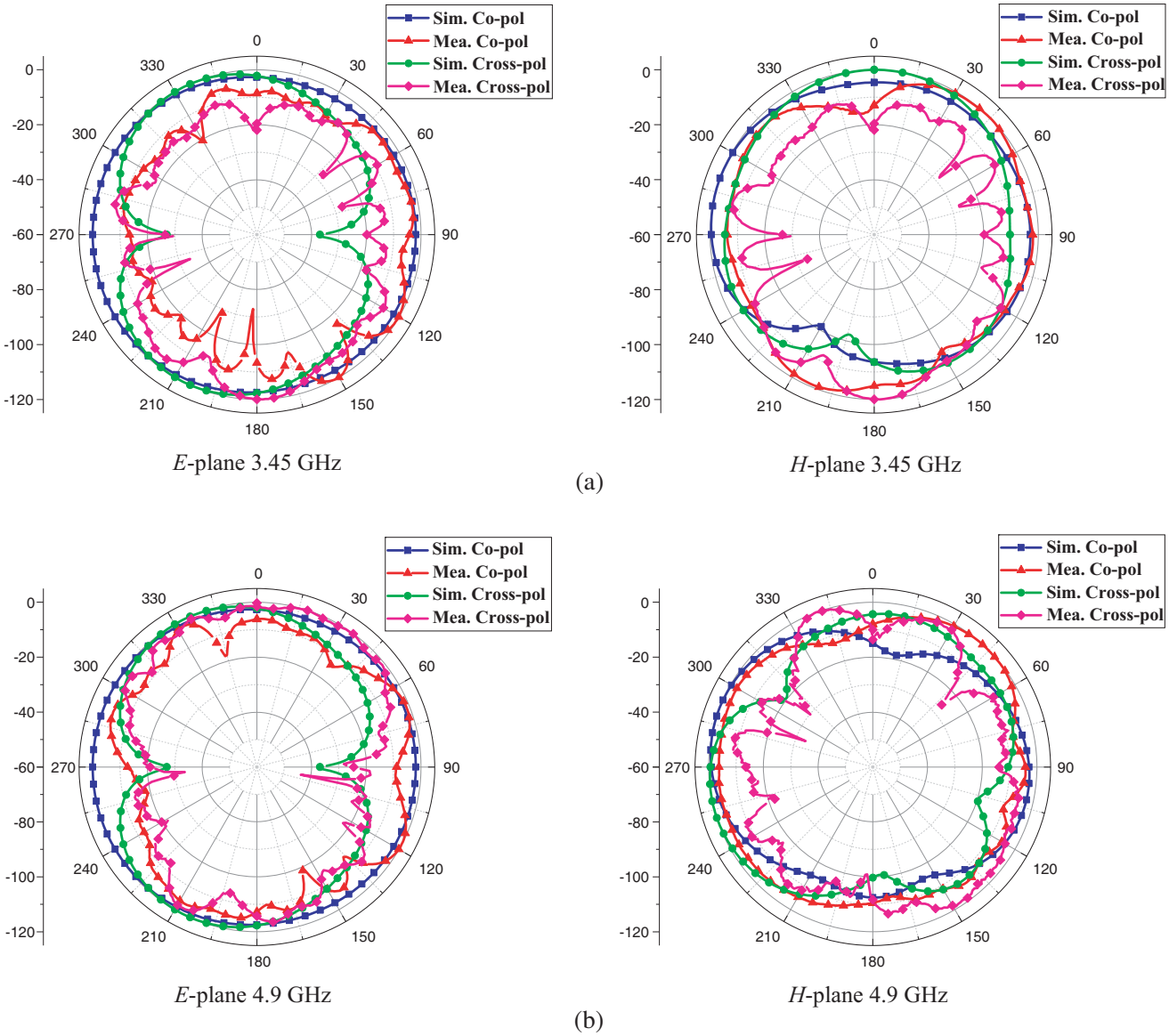


**Figure 8.** *E*-plane and *H*-plane radiation patterns of the purposed MIMO antenna at (a) 3.45 GHz and (b) 4.9 GHz.

In general, the value of CCL is defined to be below 0.4 BPS/Hz. Figure 12 plots the simulated and measured curves of CCL, which are below 0.2 BPS/Hz within operating bands. Therefore, the value of CCL can be allowed, which means that the proposed antenna can ensure a high transmission rate in the communication system.

The parameter of mean effective gain (MEG) is another significative index to measure the characteristic concerned with gain of antenna. We can evaluate MEG using the equation as given [19]:

$$\mathrm{MEG}_i = 0.5\,\eta_{i,rad} = 0.5\left(1 - \sum_{j=1}^{M} \mid S_{ij} \mid^2\right) \tag{4}$$

$$\text{Also} \quad \mid \mathrm{MEG}_i - \mathrm{MEG}_j \mid < 3\,\mathrm{dB} \tag{5}$$

where $M$ expresses the amount of antenna elements of MIMO system. Normally, the discrepancy between $\mathrm{MEG}_1$ and $\mathrm{MEG}_2$ below 3 dB can be allowed. In Figure 12, it is observed that the difference

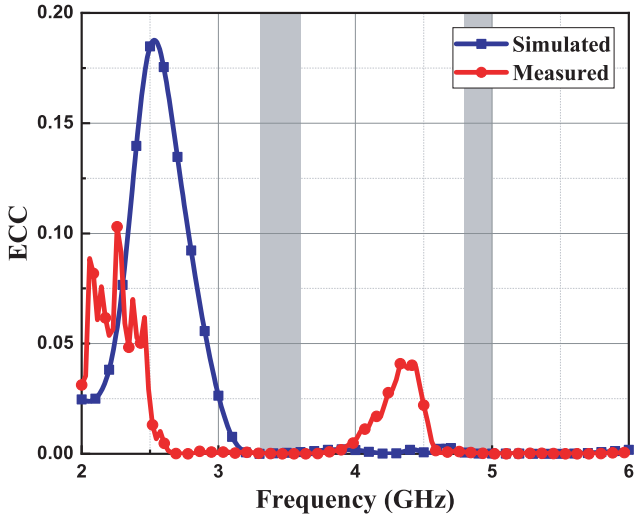


**Figure 9.** ECC of the purposed antenna.

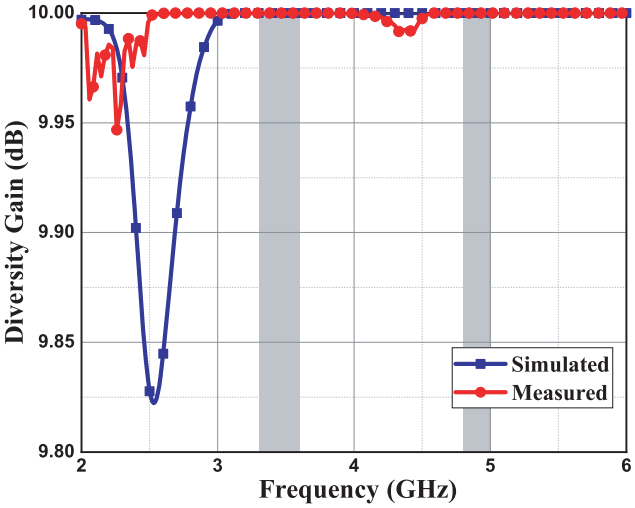


**Figure 10.** DG of the purposed antenna.

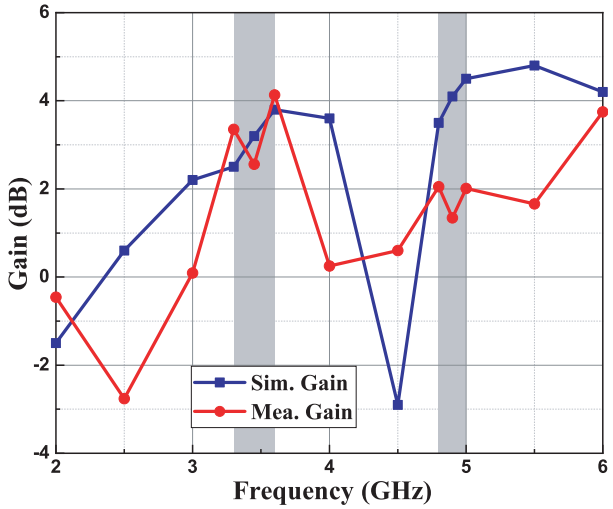


**Figure 11.** Gain of the proposed antenna.

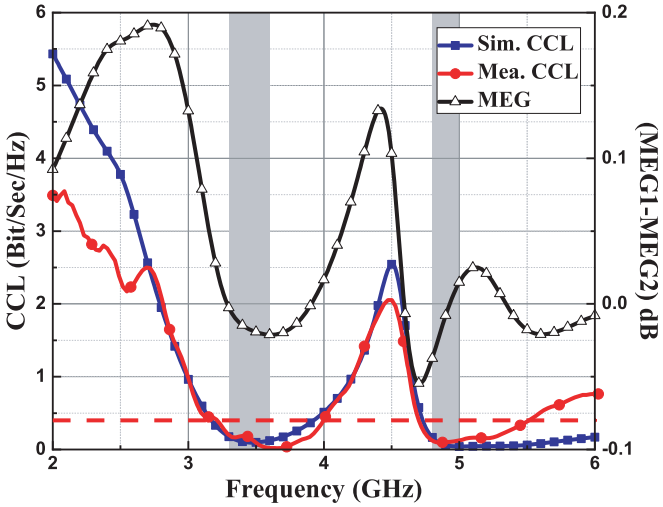


**Figure 12.** CCL and MEG of the proposed antenna.

($|\mathrm{MEG_1}\text{-}\mathrm{MEG_2}|$) is below 0.2 dB within tolerable range.

### 3.6. Total Active Reflection Coefficient

The parameter of total active reflection coefficient (TARC) represents a characteristic curve of overall reflection coefficient. With regard to a MIMO antenna with two elements, the evaluation of TARC is calculated as [20]:

$$\mathrm{TARC} = \frac{\sqrt{\left(\left|(S_{11} + S_{12}e^{j\theta})\right|^2 + \left|(S_{21} + S_{22}e^{j\theta})\right|^2\right)}}{\sqrt{2}} \tag{6}$$

where $\theta$ is denoted as the phase of excitation source, ranging from 0 to $\pi$. Figure 13 presents the curves of TARC as the variation of excitation phase angle. It can be obviously observed from the figure that the value of TARC is consistent to be less than $-10$ dB within operating bands, which shows that the proposed antenna has the possession of a good impedance match and a high isolation.

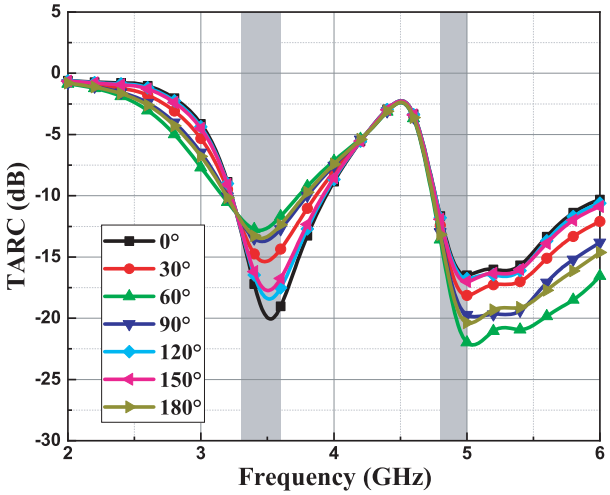


**Figure 13.** TARC of the proposed antenna.

## 4. PERFORMANCE COMPARISON

In Table 1, parameters including dimension, impedance bandwidth, minimum isolation, ECC, and feed method of the antenna in this paper are compared with some MIMO antennas reported before. It is obviously seen that the presented CPW-fed dual-band MIMO antenna has advantages with respect to overall size, isolation, and ECC. In addition, the previous antennas are generally fed by microstrip feed or coaxial feed, which will not conform to the tendency of integration and miniaturization.

**Table 1.** Performance comparison of the proposed MIMO antenna with other MIMO antennas.

| Ref. | Antenna Size ($mm^2$) | Bandwidth (GHz) | Min. Isolation (dB) | ECC | Feed Method |
|---|---|---|---|---|---|
| [3] | 3965 | 1.56–2.71, 4.82–5.9 | −15 | 0.1 | Microstrip feed |
| [4] | 3600 | 1.98–2.74, 5.19–5.74 | −25 | 0.08 | Coaxial feed |
| [5] | 4030 | 2.4–2.48, 5.15–5.825 | −15 | 0.2 | Microstrip feed |
| [6] | 3600 | 2.4–2.497, 5.15–5.94 | −20 | 0.01 | Coaxial feed |
| [7] | 2601.5 | 2.46–2.7, 5.04–5.5 | −30 | 0.01 | Coaxial feed |
| Prop. | 2114 | 3.08–3.87, 4.7–5.58 | −20 | 0.001 | CPW |

## 5. CONCLUSION

In this paper, a dual-band MIMO antenna based on CPW-feed with an enhanced isolation for 5G application is proposed. The antenna contains two antenna elements placed orthogonally and a double-Y-shaped stub printed as an isolator. The measurement results reveal that the antenna can work within operating bands covering 3.08–3.87 GHz and 4.7–5.58 GHz with the fractional bandwidth of 22.7% and 15.8%, respectively. The high isolation is better than 20 dB within 5G operating bands. The proposed antenna has a good characteristic with a rather low level of envelope correlation coefficient, a high level of DG, a reasonable gain, a high efficiency, an acceptable TARC, CCL, and MEG, and a stable radiation pattern. Therefore, the proposed MIMO antenna can be applied to 5G application.

## ACKNOWLEDGMENT

This work was supported by the National Science Foundation of China under Grant No. 61371022.

## REFERENCES


1. Zhu, Y., Y. Chen, and S. Yang, "Integration of 5G rectangular MIMO antenna array and GSM antenna for dual-band base station applications," *IEEE Access*, Vol. 8, 63175–63187, 2020.
2. Ozdemir, M. and E. Arvas, "Dynamics of spatial correlation and implications on MIMO systems," *IEEE Commun. Mag.*, Vol. 42, No. 6, S14–S19, Jun. 2004.
3. Li, Q., M. Abdullah, and X. Chen, "Defected ground structure loaded with meandered lines for decoupling of dual-band antenna," *Journal of Electromagnetic Waves and Applications*, Vol. 33, No. 13, 1764–1775, 2019.
4. Deng, J. Y., Z. J. Wang, J. Y. Li, and L. X. Gao, "A dual-band MIMO antenna decoupled by a meandering line resonator for WLAN applications," *Microw. Opt. Technol. Lett.*, Vol. 60, No. 3, 759–765, 2018.
5. Deng, J., J. Li, and L. Zhao, "A dual-band inverted-F MIMO antenna with enhanced isolation for WLAN application," *IEEE Antenna Wireless Propag. Lett.*, Vol. 16, 2270–2273, 2017.
6. Shen, D. L., L. Zhang, Y. C. Jiao, and Y. Yan, "Dual-element antenna with high isolation operating at the WLAN bands," *Microw. Opt. Technol. Lett.*, Vol. 61, No. 10, 2323–2328, 2019.
7. Liu, P., D. Sun, P. Wang, and P. Gao, "Design of a dual-band MIMO antenna with high isolation for WLAN applications," *Progress In Electromagnetics Research Letters*, Vol. 74, 23–30, 2018.
8. Luo, C., J. Hong, and M. Amin, "Mutual coupling reduction for dual-band MIMO antenna with simple structure," *Radioengineering*, Vol. 26, 51–56, 2017.
9. Nandi, S. and A. Mohan, "A compact dual-band MIMO slot antenna for WLAN applications," *IEEE Antennas Wireless Propag. Lett.*, Vol. 16, 2457–2460, 2017.
10. Qin, H. and Y. Liu, "Compact dual-band MIMO antenna with high port isolation for WLAN applications," *Progress In Electromagnetics Research C*, Vol. 49, 97–104, 2014.
11. Nirmal, P., A. Nandgaonkar, S. Nalbalwar, and R. Gupta, "A compact dual band MIMO antenna with improved isolation for WI-MAX and WLAN applications," *Progress In Electromagnetics Research M*, Vol. 68, 69–77, 2018.
12. Pasumarthi, S. R., J. B. Kamili, and M. P. Avala, "Design of dual band MIMO antenna with improved isolation," *Microw. Opt. Technol. Lett.*, Vol. 61, No. 6, 1–5, 2019.
13. Dkiouak, A., A. Zakriti, M. E. Ouahabi, and A. Mchbal, "Design of two element Wi-MAX/WLAN MIMO antenna with improved isolation using a Short Stub-Loaded Resonator (SSLR)," *Journal of Electromagnetic Waves and Applications*, Vol. 34, No. 9, 1268–1282, 2020.
14. Dkiouak, A., A. Zakriti, and M. E. Ouahabi, "Design of a compact dual-band MIMO antenna with high isolation for WLAN and X-band satellite by using orthogonal polarization," *Journal of Electromagnetic Waves and Applications*, Vol. 34, No. 9, 1254–1267, 2018.
15. Debnath, P., A. Karmakar, A. Saha, and S. Huda, "UWB MIMO slot antenna with Minkowski fractal shaped isolators for isolation enhancement," *Progress In Electromagnetics Research M*, Vol. 75, 69–78, 2018.
16. Ikram, M., Muhammad, N. Nguyen-Trong, and A. Abbosh, "Realization of a tapered slot array as both decoupling and radiating structure for 4G/5G wireless devices," *IEEE Access*, Vol. 7, 159112–159118, 2019.
17. Blanch, S., J. Romeu, and I. Corbella, "Exact representation of antenna system diversity performance from input parameter description," *Electron. Lett.*, Vol. 39, No. 9, 705–707, 2003.
18. Kumar, A., A. Q. Ansari, B. K. Kanaujia, J. Kishor, and N. Tewari, "Design of triple-band MIMO antenna with one band-notched characteristic," *Progress In Electromagnetics Research C*, Vol. 86, 41–53, 2018.
19. Kumar, A., A. Q. Ansari, B. K. Kanaujia, and J. Kishor, "High isolation compact four-port MIMO antenna loaded with CSRR for multiband applications," *Frequenz*, Vol. 72, No. 9–10, 415–427, 2018.
20. Biswas, A. K. and U. Chakraborty, "Investigation on decoupling of wide band wearable multiple-input multiple-output antenna elements using microstrip neutralization line," *International Journal of RF and Microwave Computer-Aided Engineering*, Vol. 9, 1–11, 2019.